Materials Science and Engineering A 523 (2009) 160–172

Contents lists available at ScienceDirect

Materials Science and Engineering A

journal homepage: www.elsevier.com/locate/msea

Micro-deformation mechanisms in thermoformed alumina trihydrate reinforced poly(methyl methacrylate)

E.M. Gunel*, C. Basaran[1]

Civil, Structural and Environmental Engineering, State University of New York at Buffalo, Buffalo, NY 14260, USA

ARTICLE INFO

Article history:
Received 3 April 2009
Received in revised form 22 May 2009
Accepted 28 May 2009

Keywords:
Thermoforming
Particulate reinforced composites
Scanning electron microscopy (SEM)
High-temperature deformation

ABSTRACT

Micro-deformation mechanisms involved in thermoforming of alumina trihydrate (ATH) reinforced poly(methyl methacrylate) (PMMA) was investigated in a new experimental method replicating industrial heavy-gage thermoforming procedure. Uniaxial tension tests under non-steady thermal conditions were carried out at different forming rates and forming temperatures. Stress–strain curves and load–displacement histories of thermoformed samples were studied in terms of specimen temperature at different forming conditions. Neat PMMA samples were stretched to 50% strain under identical thermoforming conditions as PMMA/ATH for comparison purposes. Stress whitening in thermoformed PMMA/ATH samples was monitored with optical microscope and degree of stress whitening was characterized by an index obtained from optical image histograms. Micro-deformation features on the surface of PMMA and PMMA/ATH samples were examined by scanning electron microscopy (SEM). Micro-deformation in neat PMMA was in the form of homogenous drawing and did not include any type of void formation. SEM images of PMMA/ATH samples showed that particle cracking is the dominant deformation mechanism at low-forming temperatures, while at high-forming temperatures, combined particle disintegration and interfacial failure are dominant mechanisms. Stress whitening was not observed in neat PMMA which was attributed to absence of micro-voids or craze-like structures. On the other hand, PMMA/ATH samples displayed different levels of stress whitening depending on density, size and type of micro-deformation features.

1. Introduction

Early implementations of thermoforming lay back to more than a century ago when celluloid sheets pressed onto steel molds. Later improvements in polymer chemistry and increasing variety of thermoformable polymer blends brought attention to this comparatively low cost and multi-system adaptable method [1]. Thermoforming is a post-processing procedure in which heated panels are stretched over or into molds by manual or pneumatic means. Typical single-stage thermoforming steps include clamping step (mechanical restraining of extruded panel in a grip device or support frame), heating step (heating of panel above glass transition temperature, T_g), shaping step (forming of heated panel to desired shape and geometry), and cooling step (cooling of formed panel to ambient temperature) [1,2]. Thermoformability which depends on thermo-mechanical and rheological properties of polymeric material is the main restriction on implementation of the procedure. Morye [3] defined different aspects of thermoformability as resistance to sag, ease of flow, mold replication, deep draw capability, sensitivity to thermoforming temperature and speed, uniformity of thickness distribution, and post-forming shrinkage and dimensional stability. Reliable estimation of thermoformability of materials and optimum thermoforming conditions are essential for the procedure. Instead of time-consuming and expensive trials on actual size panels, experimental studies on prototypes and numerical simulations of thermoforming have become more efficient techniques in evaluation of potential materials, optimization of thermoforming conditions and quality prediction of final product.

During thermoforming, heated panels can be stretched at different temperatures and rates. Typical forming rates are in the range of 0.1 and 10 s^{-1} [2]. Temperature range for thermoforming is limited between glass transition temperature (T_g) and melting temperature (T_m) of material. Amorphous polymers are in a soft rubbery state above T_g which is ideal for thermoforming. Thermoforming at temperatures close to T_m, on the other hand, may result in localized thinning and tearing of sheet. For acrylic resins, 30–40 °C above T_g was found to be ideal preheating temperature range [4]. In previous

* Corresponding author. Tel.: +1 716 698 1799; fax: +1 716 645 3733.
E-mail addresses: emgunel@buffalo.edu (E.M. Gunel), cjb@buffalo.edu (C. Basaran).
[1] Tel.: +1 716 645 2114x2429; fax: +1 716 645 3733.

0921-5093/$ – see front matter © 2009 Elsevier B.V. All rights reserved.
doi:10.1016/j.msea.2009.05.064

experimental studies for thermoforming, material characteristics were investigated while samples were in thermal equilibrium with surrounding at the beginning of thermoforming procedure, i.e. under isothermal conditions [5–7]. However, in practical thermoforming application, mold temperature (forming temperature) is lower than temperature of pre-heated sheet (sample temperature). Since sheet thickness in heavy-gage thermoforming is larger than 3 mm, thermoformed parts are exposed to significant thermal gradient. Non-uniform temperature distribution causes non-uniform thickness distribution and uneven residual stress patterns within thermoformed part [8], which may result in warpage after part is released from mold. Forming temperature and rate determine duration of cooling and amount of residual stress in thermoformed part. During forming stage, polymer chains are oriented along stretch direction. Upon cooling, they are held in position causing residual stresses. Thermoforming at high-forming temperatures requires longer cooling time and increases amount of residual stress. On the other hand, slower forming rate promotes relaxation of polymer chains and reduces amount of residual stress. Since lower residual stress results in better dimensional stability in thermoformed parts, slower forming at low temperatures are desirable [3]. However, slow forming leads to longer application periods and very low mold temperatures yields problems in appearance of thermoformed part.

Thermoforming involves different deformation modes. Stretching is essentially uniform biaxial extension in the center and nearly uniaxial extension at the clamp edge [2]. Uniaxial tension tests are often preferred to evaluate thermoformability of polymers due to experimental simplicity in application and interpretation. In biaxial stretching of polystyrene, polyethylene and polypropylene, effect of deformation mode on stress–strain curves was observed as the difference in stress level, while strain hardening behavior was similar under uniaxial stretching and biaxial stretching [9]. Film blowing and thermoforming studies on polypropylene and polyethylene also demonstrated that uniaxial elongation experiment is a versatile method for studying processing operations involving biaxial stretching [10]. Material models developed for numerical simulations commonly include material properties obtained from uniaxial tests. In numerical simulation of acrylic sheet forming, critical material properties were determined from uniaxial tension tests [11]. Thickness distribution results from numerical simulation were found in good correlation with experimental results [12].

Experimental studies on thermoformability of polymer materials and numerical simulations of thermoforming procedure have been the focus of researches in the literature. Yet, there is no study on micro-deformation mechanisms involved in thermoforming. Problems observed in appearance of thermoformed parts are related to microscopic flaws formed during the process. Thermoforming conditions strongly affect the quality and appearance of final product. In thermoforming mineral filled acrylics, stress whitening is observed as a result of excess stretching of insufficiently heated panels [13]. Therefore, it is necessary to investigate source of problems at micro level and study influence of thermoforming conditions on stress whitening. Addition of fillers improves thermal, mechanical, rheological and electrical properties of polymer matrix and lowers cost of material [14]. Primary function of soft particle inclusion is promoting matrix deformation by providing effective nucleation sites for yielding mechanisms, such as shear yielding and crazing [15]. On the other hand, reinforcement effect of rigid fillers improves strength and stiffness of polymer matrix, while ductility of polymer matrix dramatically reduces [16,17]. Rigid fillers restrict plastic deformation by increasing yield stress and modulus resulting in larger elastic regime [18–20].

Surface discoloration or enhanced opacity of polymeric materials in response to mechanical deformation is referred as “stress whitening”. Under mechanical loading, transparent or translucent polymeric materials become opaque and exhibit a whiter appearance [21], while opaque materials attain lighter color compared to original appearance [22–24]. A necessary requirement for good measurement of stress whitening is that used method should present perception of human eye. Recently, Misra et al. [25,26] developed a new method that quantifies stress whitening in terms of change in gray level obtained from optical images of deformed regions. Implementation of this method is limited to qualitative comparison of gray level change profiles of different compositions and loading conditions. In this study, optical images are further processed and single numerical values representing different levels of stress whitening are derived from image histograms. Stress whitening in PMMA based composites is primarily due to the scattering of visible light from mechanically induced surface defects, such as voids, cracks, cavities [21,27–31]. Degree of stress whitening depends on size and density of these defects and stress whitening is only observed if size of defects is in order of wavelength of visible light [20]. Stress whitening may be significantly reduced by incorporating rigid particles in polymer matrix such that plastic deformation is minimized [19,22,25,26,32]. However, inadequate interfacial bonding strength may result in micro-void formation and further enhance stress whitening in particle filled polymers. In such cases, source of stress whitening is void formation due to debonding of particles from matrix and/or breaking of particles [33–36].

Inclusion of rigid particles in polymer matrices results in different failure behavior depending on particle size and concentration [37–41], interfacial bonding strength [33,42], relative matrix and filler strength [24,35,43]. The effect of particle size on mechanical properties of composites is related to specific surface of particulates. Large specific surface of small particles enhances bonding with matrix and improves reinforcement effect. Yet, blending polymers with very small particles results in agglomeration and non-uniform dispersion which are both detrimental to mechanical properties of composite [38,39]. The strength of interphase modifies stress distribution in the vicinity of filler and promotes different failure mechanisms. In general, strong interfacial bonding improves strength and stiffness of bulk material in the expense of ductility, while weak interfacial bonding reduces mechanical properties along with improved toughness [44]. Surface treatment on particles in the form of chemical agents may improve adhesion between matrix and particles. Coupling agents form strong bond between filler and matrix which results in uniform particle dispersion and increase in yield stress and stiffness, yet strong interfacial adhesion reduces deformation capacity. [33]. In a recent study, effect of surface treatment on tensile deformation behavior of ATH filled PMMA was investigated [45,46]. In composites with adhesion promoting additives, reinforcement effect of particles were more pronounced compared to composites without chemical agent and composites with debonding agent. Adhesion promoters resulted in higher tensile strength but lower toughness in tensile testing of PMMA/ATH. Fracture of particulate composites also depends on relative stiffness and strength of constituent materials and interface strength. If both constituent materials have material properties in the same order, particle cracking occurs. If embedded particles are much stiffer and stronger than matrix, particle debonding or matrix tearing becomes major damage mode.

In the present work, a new experimental method has been proposed for heavy-gage thermoforming procedure with specific emphasis on non-steady thermal condition for specimens during forming stage. Influence of forming rate and temperature on material response throughout all stages of thermoforming procedure has been studied. Micro-deformation mechanisms in thermoformed mineral filled acrylics have been investigated with scanning electron microscopy.

2. Experimental procedure

2.1. Materials

Standard ASTM D638 Type IV specimens [47] from extruded acrylic (PMMA) and acrylic particulate composite (PMMA/ATH) panels [48] were used for experimental study. ASTM D638 Type IV specimens are suggested for direct comparison between materials in different rigidity cases, similar to thermoforming procedure in which material undergoes a transformation from non-rigid to rigid form around its T_g. Acrylic particulate composite in this study is characterized by ductile properties of lightly cross-linked, low-molecular weight PMMA and hard, brittle nature of ATH. According to supplier provided information, PMMA has a T_g around 100 °C which was obtained from differential scanning calorimetry test. The number-average molecular weight (M_n) of PMMA was determined as 150 kg/mol from batches without cross-linking agent. ATH inclusion in PMMA specifically improves dimensional stability and flame resistance of polymer matrix. Primary function of ATH as a fire retardant agent is ignition inhibitor by increasing ignition temperature and forming incombustible gases in the flame zone. ATH fillers also act as smoke suppressants by catalyzing oxidation of carbonaceous matter on burning surface [49]. Inclusion of ATH fillers results in better high-temperature performance in the expense of reduction in ductility.

Average particle size of ATH is 30–40 μm and particle volume fraction in acrylic composite is 50%. ATH agglomerates are irregular in shape and they are strongly bonded to PMMA matrix by means of adhesion promoting agent [46]. Another important aspect of acrylic particulate composite is the temperature at which thermal micro-stresses around ATH particles disappears. Thermal micro-stresses due to coefficient of thermal expansion (CTE) mismatch between filler/matrix can be monitored by utilizing stress optically birefringence characteristic of PMMA. For PMMA/ATH in this study, it was found that stress field around agglomerates disappeared when sample was heated to 90 °C [45]. Sun and Liu [50] showed that fabrication cooling process causes plastic flow of the composites and overall yield surfaces of the composites exhibit a combination of kinematic and isotropic plastic hardening in the presence of thermal stresses due to CTE mismatch. Upon cooling, stress level around fillers may reach 15–75% of tensile yield strength of composite. Therefore, thermal micro-stress due to CTE mismatch plays an important role in the failure of particulate composites under thermo-mechanical loading conditions.

2.2. Thermoforming experiments

Uniaxial tension tests are often preferred for evaluation of thermoforming performance of materials due to experimental simplicity in application and interpretation [5–7,10]. Material models developed for thermoforming simulation commonly include material properties obtained from uniaxial tests [11,12]. Based on these observations, uniaxial tensile stretching of samples was preferred in place of industrial heavy-gage thermoforming procedure. Similar to standard thermoforming procedure, samples were first heated to a temperature above T_g using VWR Signature™ Horizontal Airflow type convection oven. Ideal pre-forming temperature for PMMA is estimated as 30–40 °C above T_g [4]. Heating duration and pre-forming temperature were established as 20 min and 150 °C on the basis of manufacturer's manual. For continuous monitoring of specimen temperature during testing, temperature of the specimens was recorded by using OS-PP Omegaette™ Pocket Pal® infrared thermometer at intervals. Test procedure for thermoforming is considered mainly in three steps: first, loading step corresponding to forming step; second, dwell step corresponding to cooling step; and third, unloading step corresponding to removal of sample from mold. Loading history of thermoforming test is presented in Fig. 1.

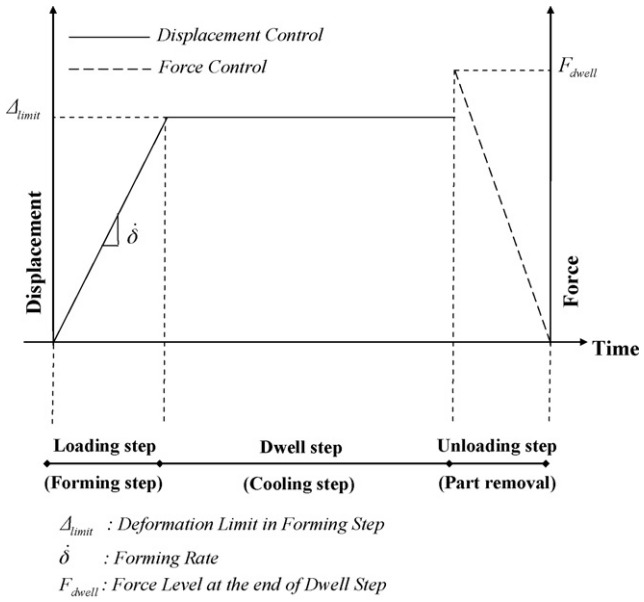

Fig. 1. Loading history of thermoforming procedure.

Displacement controlled testing was preferred in the forming step, since it was not possible to use any form of strain measurement device. In a soft malleable state, samples were not able to withstand the weight of axial extensometer. Strain gages are not suitable for large strain measurements (>5%) at high temperatures (>100 °C), whereas laser sensors are not advised for high-temperature applications. Heated specimens were stretched to different levels of deformation in a servomechanical MTS material testing unit type 858 table top system (1–10 kN capacity) controlled by a computer and fitted with an ATS 7510 box thermal chamber for the control of ambient temperature. In order to prevent extrusion of material from grips, minimum possible grip pressure was employed. Grip slip was not observed due to special serration pattern on grip wedges. Initial distance between grips was kept at minimum possible level such that uniaxial stretching was confined to the neck-down portion of the dogbone sample [2]. Strain values in engineering stress–strain curves were calculated by dividing crosshead displacement by gauge length. Forming rate was chosen at three different displacement rates as 0.9, 0.09, 0.009 mm/s (equivalent strain rate of $\sim 10^{-2}$, $\sim 10^{-3}$, $\sim 10^{-4}$ s^{-1}, respectively). Although typical thermoforming rates are in the range of 0.1–10 s^{-1} [2], scale effect on specimen size substantially restricted applicable strain rate in thermoforming tests. Forming temperatures representing different mold temperatures were selected as 30, 50, 75, 90, 100, 125, and 140 °C. Results presented herein are the arithmetic average of results obtained from five separate tests conducted at the same condition.

During forming step, temperature was held fixed in thermal chamber representing desired mold temperature. Deformation limits in forming step were established as 4.5, 6.75, 9, 13.5 and 18 mm. Samples were thermoformed for five times with increasing deformation level in each subsequent thermoforming cycle. Successive thermoforming applications on the same sample were planned to investigate damage evolution in repeated thermoforming cycles. At the beginning of dwell step, thermal chamber door was opened for cooling of sample. During dwell step, specimen deformation was held fixed. Time necessary for cooling was established between 1.5 and 8 min depending on forming temperature. Unloading at high rate was preferred in order to characterize rapid removal of thermo-

formed part from the mold. During thermoforming tests, ambient temperature, upper and lower grip temperatures and surface temperature of samples were continuously recorded. In addition to thermoforming tests, PMMA/ATH samples were tested to failure and PMMA samples were stretched to ~50% strain under identical thermoforming testing conditions. Test results of PMMA samples are not presented in this paper.

2.3. Scanning electron microscopy

Micro-deformation features on the surface of thermoformed PMMA/ATH samples and influence of forming rate and temperature on micro-deformation mechanisms were studied using scanning electron microscopy (HITACHI S4000) in secondary electron imaging mode. PMMA samples stretched to ~50% strain were also examined for comparison purposes. All samples were cryofractured at the ends without damaging thin mid-portion and carbon coated prior to examination.

2.4. Stress whitening characterization

Stress whitening characterization of thermoformed PMMA/ATH samples is based on the difference in appearance at virgin and thermoformed state. Specimens were monitored with Panasonic GPKR222 CCD camera before any test (virgin state) and at the end of each thermoforming cycle (thermoformed state). A region of 2 mm × 2.5 mm in the middle of specimen was examined at all cases. Great care was taken to maintain same brightness level in all optical images. Optical images were first converted to gray mode from RGB mode using Adobe® Photoshop® software. Processed images were then digitized using MatLAB® Image Processing Toolbox™ software and image histograms were obtained in gray scale. An index corresponding to appearance of monitored region was derived from image histograms. Finally, stress whitening in thermoformed samples was numerically defined as the difference between indices of virgin and thermoformed state.

3. Results and discussion

3.1. Mechanical properties

In simple uniaxial tensile tests of PMMA/ATH, specimens were stretched at different temperatures and rates until the failure of specimen. Engineering stress–strain curves of PMMA/ATH samples tested to failure are presented in Fig. 2. Similar to thermoforming tests, specimens were heated to 150 °C prior to testing. Unlike standard isothermal testing of materials, specimen temperature in H and M series tests (tests at 0.9 and 0.09 mm/s displacement rate) was not constant and specimens were not in thermal equilibrium with surrounding ambient. While specimens were stretched to failure, they were also cooling down to environmental chamber temperature (or mold temperature). This situation is identical to industrial heavy-gage thermoforming procedure during which panels start cooling immediately at forming stage. On the other hand, at 0.009 mm/s forming rate (L series tests), specimen temperature was nearly constant through testing. Displacement rate and test temperature in these tests will be henceforth referred as forming rate and forming temperature.

At high-forming temperatures ($T > 100$ °C), stress–strain relationships for all forming rates can be characterized with a yield stress followed by a huge yield plateau without strain hardening behavior. At low-forming temperatures ($T < 100$ °C), stress–strain relations strongly depend on the competition between forming rate and cooling rate. Cooling rate depends on the difference between specimen temperature and forming temperature, and cooling is much faster at low-forming temperatures. If forming rate is higher

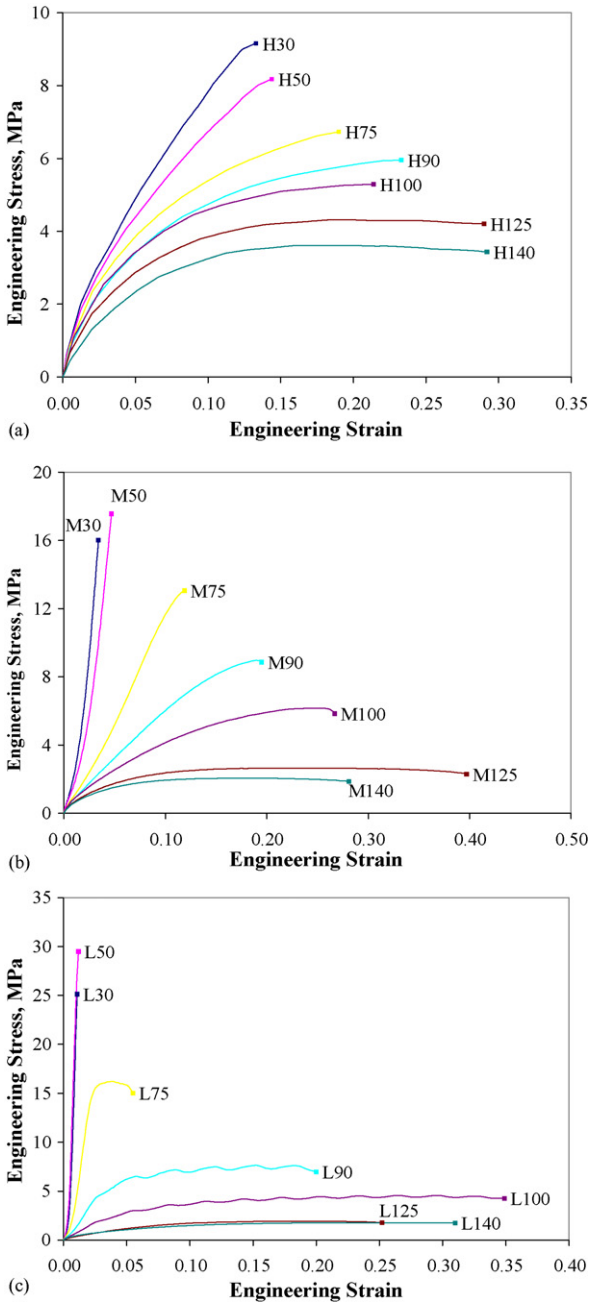

Fig. 2. Engineering stress–strain curves of PMMA/ATH samples tested to failure at: (a) 0.9 mm/s, (b) 0.09 mm/s and (c) 0.009 mm/s displacement rates.

than cooling rate (H series tests), specimen temperature is always larger than forming temperature. If forming is slower than cooling (L series tests), specimens completely cool down to forming temperature. Therefore, for forming temperatures below 100 °C, specimen temperature in H series (0.9 mm/s forming rate) was higher than that in M series tests (0.09 mm/s forming rate), whereas at 0.009 mm/s forming rate (L series tests), specimens always reached thermal equilibrium before test completion and had the lowest temperature. Since cooling at forming temperatures above 100 °C is insignificant, samples were stretched at nearly constant temperature regardless of forming rate. As a result, at forming temperatures below 100 °C, ultimate strength and tensile modulus decrease with increasing forming rate, while at forming temperatures above 100 °C, ultimate strength increases as forming rate increases. Similarly, at forming temperatures below 100 °C, varia-

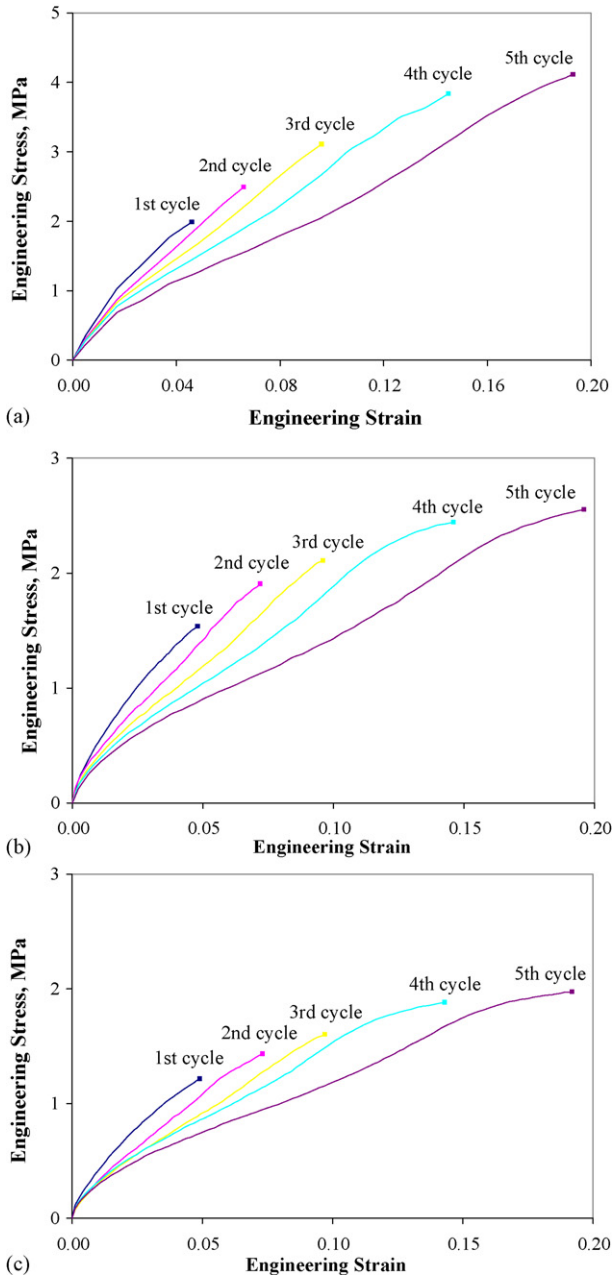

Fig. 3. Engineering stress–strain curves of PMMA/ATH samples in forming step (a) at 0.9 mm/s forming rate, 90 °C forming temperature. (b) At 0.09 mm/s forming rate, 125 °C forming temperature. (c) At 0.009 mm/s forming rate, 125 °C forming temperature.

tion of modulus with forming temperature is more remarkable in L and M series tests, while at temperatures above 100 °C, this variation is more noticeable in H series test. Yet, for all forming rates, as forming temperature decreases, elongation at failure decreases while tensile strength and modulus increase.

Engineering stress–strain curves for the forming step at selected thermoforming conditions (H90, M125 and L125 series) are presented in Fig. 3. At all thermoforming conditions, stress–strain curves in the first forming cycles are similar to initial 5% strain portion of curves in tensile tests to failure (Fig. 2). This observation was anticipated because in the first thermoforming cycle and "to failure" tests, virgin samples were stretched for the first time under the same conditions. Repeated thermoforming cycles on the same sample, on the other hand, cause deviation from first cycle

Table 1
Number of possible thermoforming cycles before failure of PMMA/ATH samples at different conditions (na: not applicable).

Number of cycles		Forming temperature (°C)						
		30	50	75	90	100	125	140
Forming rate (mm/s)	0.9	3	4	4	5	5	5	5
	0.09	na	1	3	4	5	5	5
	0.009	na	na	1	3	5	5	5

stress–strain curve because of damage evolution in material (Fig. 3). Stress values corresponding to same strain at sequential thermoforming cycles gradually decrease because of strength and stiffness degradation. The amount of irreversible damage introduced in material varies with forming temperature and rate. Damage evolution with successive thermoforming cycles also limits possible number of thermoforming operation on PMMA/ATH specimens especially at low temperatures. Number of thermoforming cycles before failure of PMMA/ATH samples at different conditions is presented in Table 1. At some thermoforming conditions (M30, L30 and L50), thermoforming testing was not possible because elongation at break in simple uniaxial tension tests were less than 4.5 mm which was defined as the deformation limit in the first thermoforming cycle (Fig. 2b and c).

Heat application at the beginning of each thermoforming cycle was another factor affecting material performance in thermoforming tests. At this stage, plastic deformation in the polymer matrix alone was recovered similar to polymer healing upon heat treatment, while damage in the ATH agglomerates and in the interphase were not recovered. Strength degradation in stress–strain curves clearly indicates that complete healing did not occur, though specimens were heated to 150 °C between thermoforming cycles. Healing process at elevated temperatures beyond T_g of material involves restoration of secondary bonds between mobilized polymer chains and transportation of severed chains by a diffusional process [51]. By means of this healing process prior to testing, the part of damage associated with polymer matrix was reversed to some extent and composite strength and stiffness at early stages of deformation (for strain values less than 2%) did not change significantly with increasing number of thermoforming cycles. Material degradation was only pronounced at high-strain levels where increasing damage in mineral fillers cause noticeable change in stiffness and strength.

Typical loading–displacement histories of thermoforming tests are presented in Fig. 4. Following forming step, environmental chamber door was opened and specimens were left for cooling at room temperature while deformation at the end of forming step was kept constant during cooling period. In cooling step, behavior of PMMA/ATH samples is governed by two counter-acting phenomena. At the beginning of dwell step, stress values drop by some amount because of stress relaxation of polymer matrix whereas continuous cooling increases tensile stress in the sample induced by thermal shrinkage at constant deformation level. The competition between stress relaxation and thermal stress determines maximum experienced tensile stress throughout thermoforming procedure. The effect of stress relaxation is more pronounced at high-forming rates while effect of thermal stress is more pronounced at high-forming temperatures. If forming temperature is below 90 °C, regardless of forming rate, maximum experienced stress occurs in the forming step, i.e. effect of thermal shrinkage at these temperatures is less pronounced upon sufficient cooling in forming step. For temperatures above 90 °C, maximum experienced stress occurs at the end of cooling step and may have a value twice as much as maximum stress in forming step. At 0.9 mm/s forming rate, as forming temperature increases, amount of stress

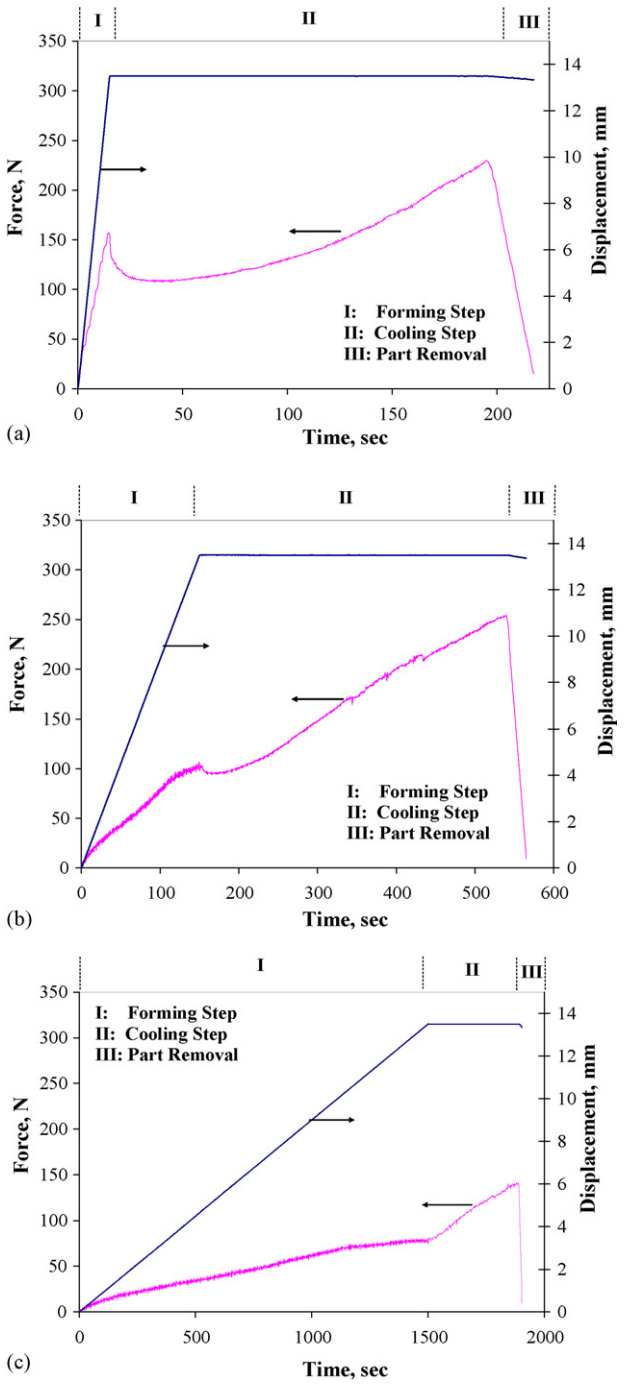

Fig. 4. Loading–displacement history of PMMA/ATH sample thermoformed (a) at 0.9 mm/s forming rate, 90 °C forming temperature. (b) At 0.09 mm/s forming rate, 125 °C forming temperature. (c) At 0.009 mm/s forming rate, 125 °C forming temperature (deformation limit 13.5 mm).

relaxation decreases and duration of stress relaxation increases. At 0.09 mm/s forming rate, amount and duration of stress relaxation is smaller compared to 0.9 mm/s forming rate. At 0.009 mm/s forming rate, there was no noticeable stress relaxation, since at such low loading rate, there was sufficient time for molecular relaxation before any additional load increment during forming step. In unloading step, elastic recovery takes place to different extent depending on forming rate and temperature, yet recovered elastic strain is less than 0.1% of total strain at all thermoforming conditions.

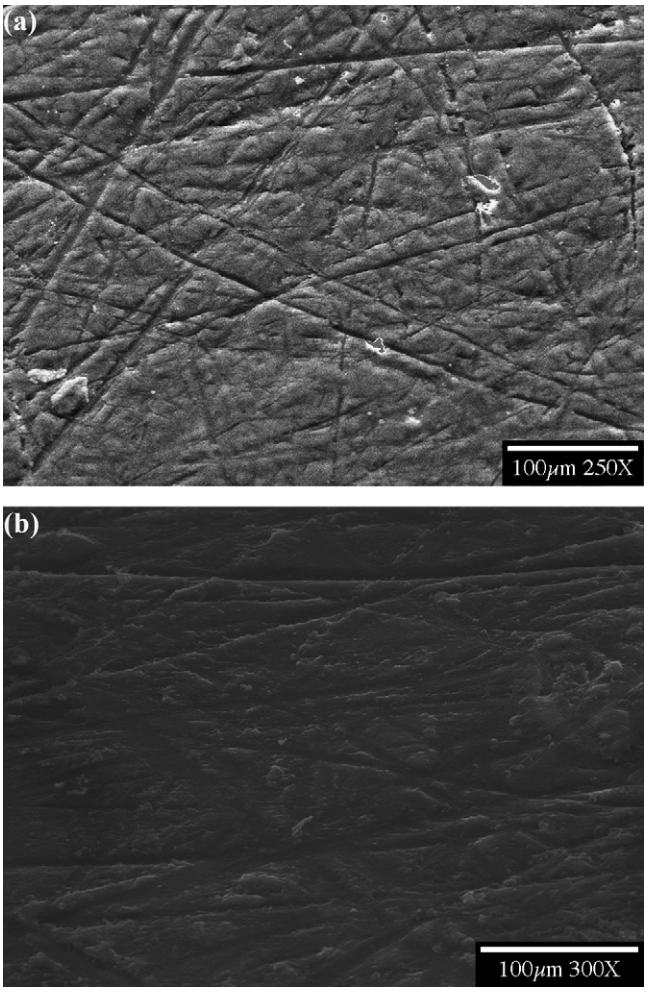

Fig. 5. SEM images of (a) undeformed PMMA sample and (b) PMMA sample stretched to ~50% strain at 100 °C and 0.9 mm/s displacement rate.

3.2. Micro-deformation mechanism in thermoformed acrylics

In our experimental study, stress whitening was only observed in thermoformed PMMA/ATH samples, while PMMA samples did not display any stress whitening at any testing condition. Surface features were studied in order to investigate source of stress whitening in thermoformed PMMA/ATH samples. In addition, neat PMMA samples were investigated, since at micro-level, deformation characteristics of neat polymer and its composites are usually interrelated.

3.2.1. Surface deformation in neat PMMA samples

Surface structure of undeformed PMMA sample (Fig. 5a) displays large amount of scratches formed during sample preparation. SEM image of stretched PMMA sample (Fig. 5b) clearly shows that there is no micro-void formation on the surface and original surface texture was preserved during homogeneous plastic deformation of polymer in the form of enlargement of previously formed scratches. In the absence of micro-voids or other light scattering entities, PMMA samples did not display any stress whitening under any thermoforming conditions. Previous studies on PMMA indicated that source of stress whitening in neat PMMA was micro-void formation due to crazing [52,53] and that in rubber modified PMMA was due to cavitation or debonding of rubber particles [27,28,31,54]. In our case, PMMA molecular structure was modified with cross-linking agent in order to improve stiffness and strength of the material. Resulting molecular network restricts polymer chain mobility and

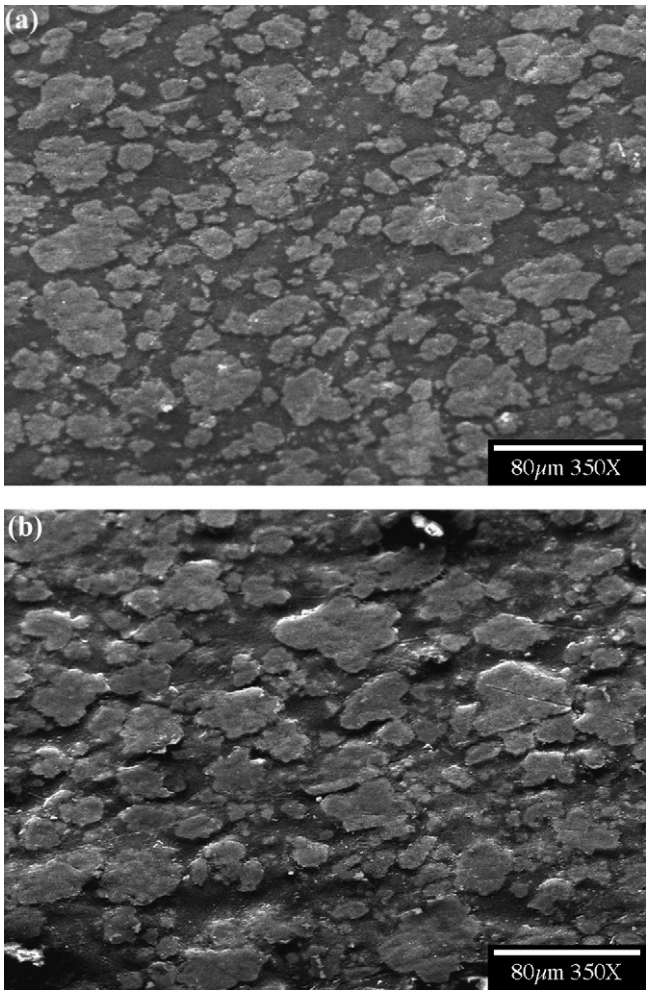

Fig. 6. SEM images of (a) undeformed PMMA/ATH sample and (b) virgin PMMA/ATH sample heated at 150 °C for 20 min.

reduces possibility of fibrillation which is a primary condition for craze widening or thickening. In addition, for a stable craze growth in PMMA, critical number-average molecular weight (M_c) was found as 200 kg/mol based on experimental studies [55]. Since PMMA in our study has a molecular weight (M_n = 150 kg/mol) less than the critical value, it is unlikely to observe a craze structure in neat PMMA. Finally, PMMA samples were stretched at temperatures above T_g where micro-deformation mechanism generally does not involve crazing or shear yielding but it is in the form of homogenous drawing of bulk polymer [56].

3.2.2. Surface deformation in thermoformed PMMA/ATH samples

SEM image of undeformed PMMA/ATH sample is presented in Fig. 6a. It is clear that particle size distribution of ATH fillers is quite large and ATH agglomerates are randomly dispersed in PMMA matrix. In order to examine the effect of heating on surface texture of PMMA/ATH, a virgin sample heated at 150 °C for 20 min was investigated (Fig. 6b). It is apparent that heating prior to thermoforming procedure does not cause any loss of mechanical integrity between PMMA and ATH, yet surface finishing layer applied during sample preparation disintegrates by heat application which reveals the level difference between filler and matrix causing slight change in optical appearance of composite.

Recently, Basaran et al. studied tensile behavior of PMMA/ATH samples with different interfacial strength [42]. Strong interfacial bonding strength was achieved by treating ATH agglomerates with adhesion promoting chemical agents, whereas debonding promoting agent was used for eliminating any possible chemical bond between polymer and matrix. It was observed that difference in tensile behavior of different blends arises from failure mechanisms at micro-level [42]. Failure in composite with adhesion promoting additives was internal cracking of ATH agglomerates while debonding of particles from matrix took place in composite with debonding promoting additives. In the acrylic composite used in this study, ATH agglomerates are strongly bonded to PMMA matrix. SEM images of thermoformed samples show that nature of deformation in polymer matrix significantly changes with respect to forming temperature and rate leading to different modes of particle failure.

Surface deformation features associated with stress whitening was studied on samples from last available thermoforming cycles. SEM images of PMMA/ATH samples thermoformed at 0.9 mm/s forming rate and at different forming temperatures are presented in Fig. 7. SEM images show that main failure mechanism at temperatures below T_g of PMMA (100 °C) is particle cracking and at temperatures above 100 °C, it is combined interfacial failure and particle disintegration with ductile tearing of matrix. However, main source of stress whitening in all cases is light scattering entities formed by failure of ATH agglomerates. At 0.9 mm/s forming rate, intensity of particle cracking at 75 °C forming temperature (Fig. 7c) is less compared to 50 °C forming temperature (Fig. 7b). Since influence of thermal stress due to CTE mismatch diminishes as temperature increases, thermal micro-stress field around ATH particles also reduces and particle failure also decreases at 75 °C forming compared to 50 °C forming. At 90 °C forming temperature (Fig. 7d), intensity of particle cracking is more than that at 75 °C forming temperature (Fig. 7c). As forming temperature increases, polymer matrix becomes more flexible while ATH remains rigid regardless of forming temperature since ATH has a melting temperature around 3500 °C. At 90 °C forming temperature, polymer matrix is also still stiff enough to exert large tensile stresses on ATH particle such that resultant state of stress causes failure of ATH particles at a higher level compared to that at 75 °C. Since at 0.9 mm/s forming rate, specimen temperature is higher than forming temperature, transition in polymer matrix characteristics was observed at 90 °C forming temperature. At 100 °C forming temperature, polymer chain mobility increases significantly and strength and stiffness of PMMA matrix reduce dramatically. Severe deformation in matrix causes failure only at particle-matrix interphase or some weak particles (indicated with arrows in Fig. 7e), such that it is sufficient enough to permit large deformation of polymer matrix while major portion of particles remain intact. At 125 °C forming temperature, source of micro-deformation mechanism is completely different than colder forming temperatures. At this forming temperature, matrix is more like in a semi-liquid form. Severe stretching of highly mobilized polymer chains leads to failure in particle-matrix interphase, observed as isolated large size particles in Fig. 7f. On the other hand, small size ATH agglomerates fails at many locations causing formation of fine cracks (Fig. 7f) contrary to previous cases where single cracks were observed. Further increase in forming temperature causes disintegration of ATH agglomerates (encircled in Fig. 7g) because of completely incompatible deformation capabilities of the two constituents while interfacial failure is still observable at some isolated large particles.

SEM images of PMMA/ATH samples thermoformed at 0.09 mm/s forming rate and at different forming temperatures are presented in Fig. 8. At 0.09 mm/s forming rate, matrix deformation is not significant for forming temperatures below T_g of PMMA and failure of ATH particles are controlled by the level of thermal stress due to CTE mismatch. Only at forming temperatures above 100 °C, polymer matrix deformation controls intensity of particle cracking. Density of cracks at 100 °C thermoforming (Fig. 8c) was increased

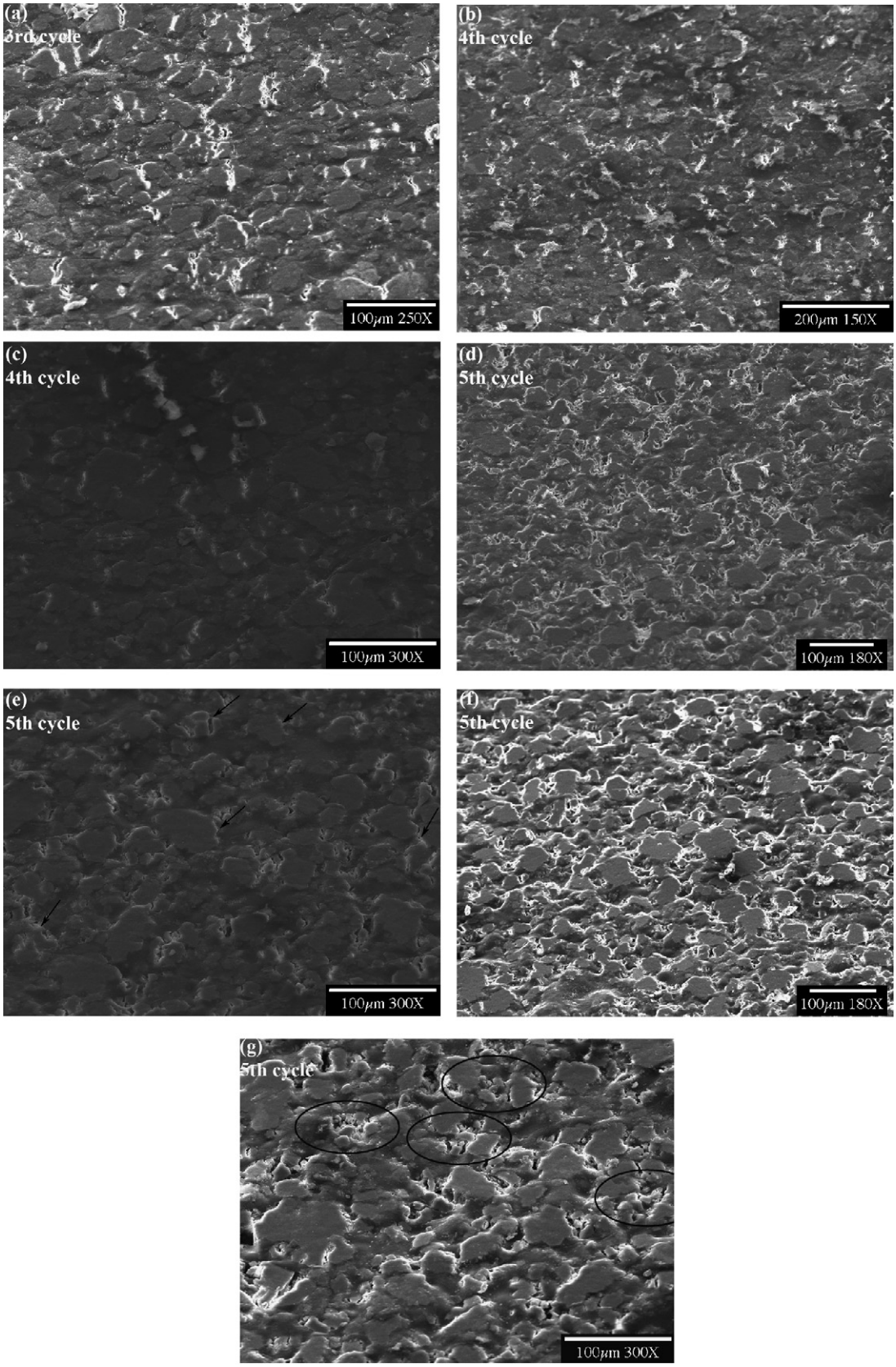

Fig. 7. SEM images of thermoformed PMMA/ATH samples at 0.9 mm/s forming rate at (a) 30 °C, (b) 50 °C, (c) 75 °C, (d) 90 °C, (e) 100 °C, (f) 125 °C and (g) 140 °C forming temperatures.

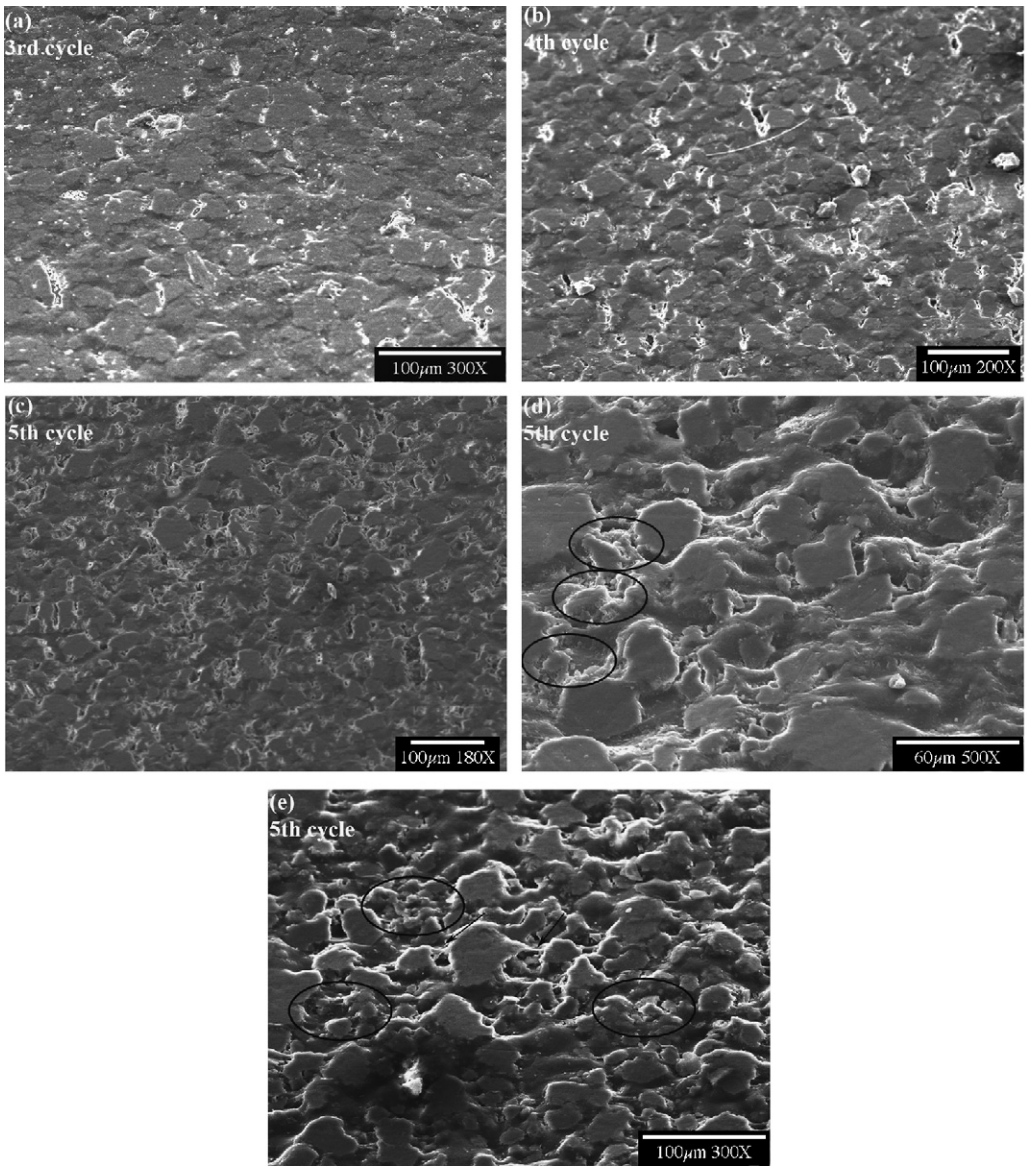

Fig. 8. SEM images of thermoformed PMMA/ATH samples at 0.09 mm/s forming rate at (a) 75 °C, (b) 90 °C, (c) 100 °C, (d) 125 °C and (e) 140 °C forming temperatures.

significantly compared to lower forming temperatures (Fig. 8a and b). Increase in intensity of light scattering entities is attributed to change in polymer matrix behavior from solid to semi-fluid like behavior. At 100 °C forming temperature, ATH fillers are prone to cracking at a higher level, because surrounding highly mobilized polymers have a tendency of flowing rather than deforming coherently with agglomerates (Fig. 8c). At even higher forming temperatures (125 and 140 °C), this flow-type deformation mechanism becomes more obvious. As surrounding polymer matrix flows (stretches) around fillers, ATH agglomerates disintegrate instead of cracking (encircled in Fig. 8d and e). Isolated large particles in Fig. 8d and e indicates that interfacial failure is significant at 125 and 140 °C forming temperatures. Since 0.09 mm/s forming rate is relatively faster than relaxation rate, tearing of highly stretched polymer chains around ATH fillers was also observed (indicated with arrows in Fig. 8e). At 0.09 mm/s forming rate, particle disintegration also took place at 125 °C forming temperature (Fig. 8d), contrary to the case at 0.9 mm/s forming rate.

SEM images of PMMA/ATH samples thermoformed at 0.009 mm/s forming rate and at different forming temperatures are presented in Fig. 9. At 0.009 mm/s forming rate, particle cracking is only observed at 75 and 90 °C forming temperatures and intensity of particle cracking depends on the level of thermal stress around ATH particles (Fig. 9a and b). Deformation in polymer matrix is only severe at temperatures above 90 °C. Ductile stretching of polymer matrix takes place which is accompanied with particle disintegration (encircled in Fig. 9c–e). Transition in polymer behavior at 100 °C forming temperature can be also observed at 0.009 mm/s forming rate (Fig. 9c) similar to that in 0.09 mm/s forming rate (Fig. 8c). Severe plastic deformation in polymer matrix causes formation of large size cracks in ATH agglomerates at 100 and 125 °C forming temperatures. On the other hand, sufficient relaxation in highly stretched polymer chains reduces severity of failure of polymer matrix at 140 °C forming temperature. Increase in surface irregularity at high-forming temperatures (100, 125 and 140 °C) also hinders stress whitening to some extent because light is scattered into many directions from irregular surfaces [35,57]. Similarly, large size voids or cavities (at 100 and 125 °C forming temperature) also absorb light instead of scattering which results in lower stress whitening level [19,32].

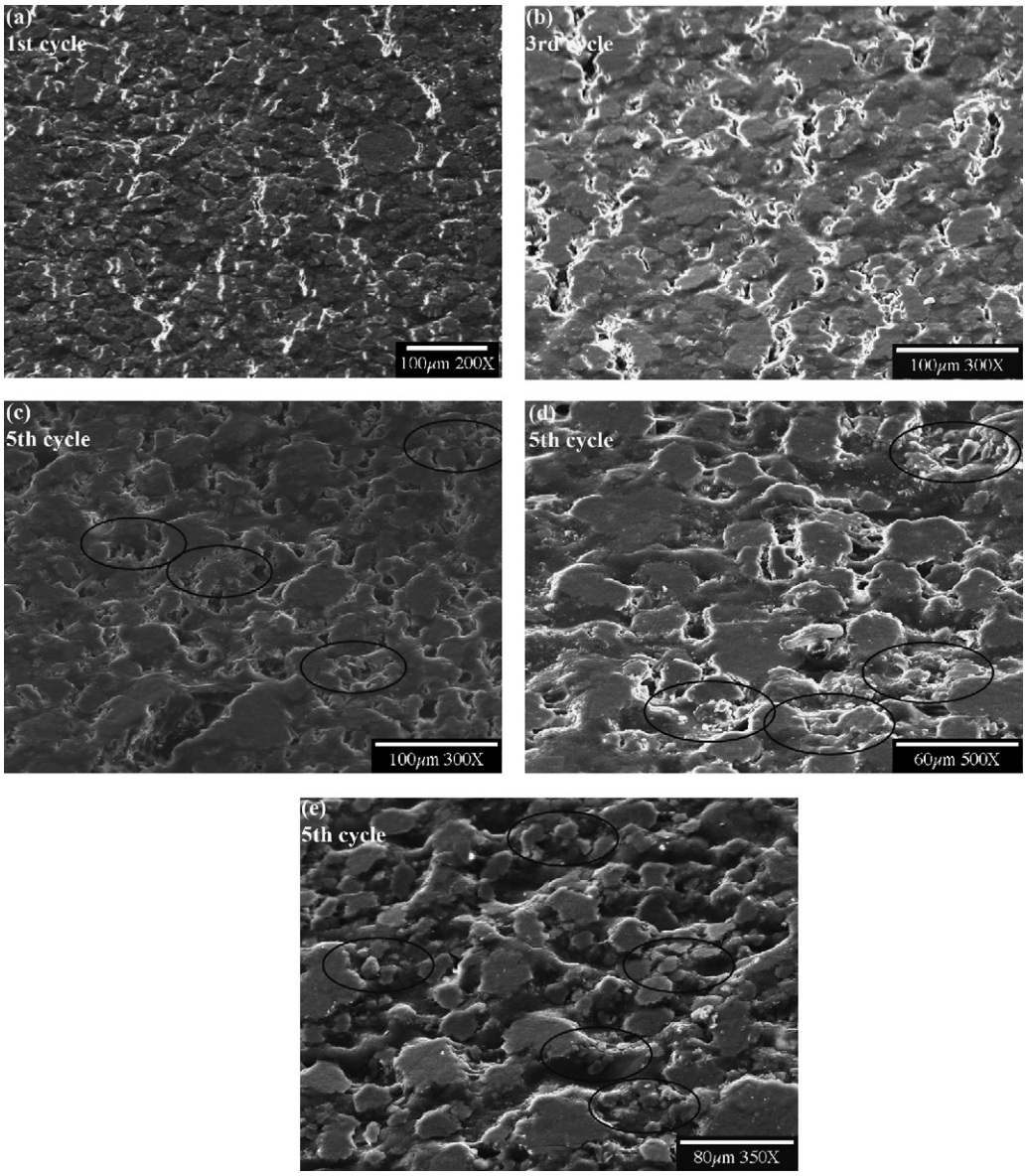

Fig. 9. SEM images of thermoformed PMMA/ATH samples at 0.009 mm/s forming rate at (a) 75 °C, (b) 90 °C, (c) 100 °C, (d) 125 °C and (e) 140 °C forming temperatures.

Absence of crazing yielding mechanism in PMMA/ATH samples can be attributed to homogenous high-temperature deformation of cross-linked, low-molecular weight polymer matrix which was discussed in stretching of PMMA. In addition, it was observed in particulate reinforced composites with high volume fraction that small interparticle distance yields overlapping stress fields which prevent crazing formation [58,59]. Under such conditions, it is clear that a stable craze structure cannot be formed in PMMA and PMMA/ATH samples.

In order to study the influence of healing upon heat treatment prior to thermoforming cycles, a PMMA/ATH sample was heated after the 5th thermoforming cycle at 0.9 mm/s forming rate and 100 °C forming temperature. SEM image of post-heated PMMA/ATH sample is presented in Fig. 10. Compared to image in Fig. 7e, it is clear that cracks in ATH agglomerates are closed mostly while failure zones are still observable within fillers and at matrix-filler interphase (indicated with arrows in Fig. 10). Such defects in post-heated PMMA/ATH sample are the sources of residual stress whitening. However, intensity of remaining flaws is very small compared to density and size of fully developed cracks in a

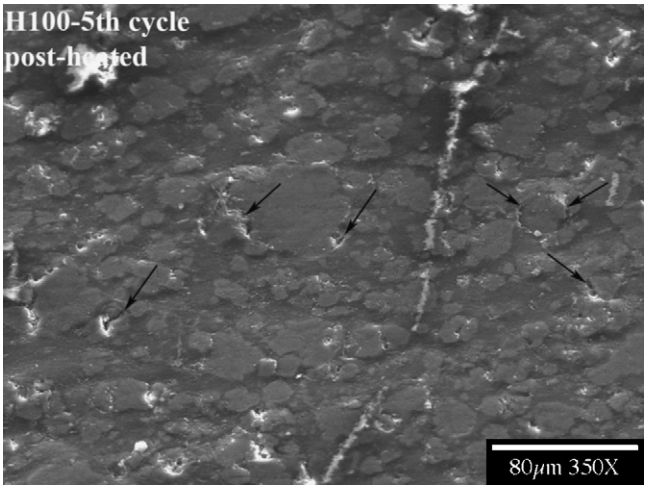

Fig. 10. SEM image of post-heated PMMA/ATH sample after thermoformed at 0.9 mm/s forming rate and 100 °C forming temperature.

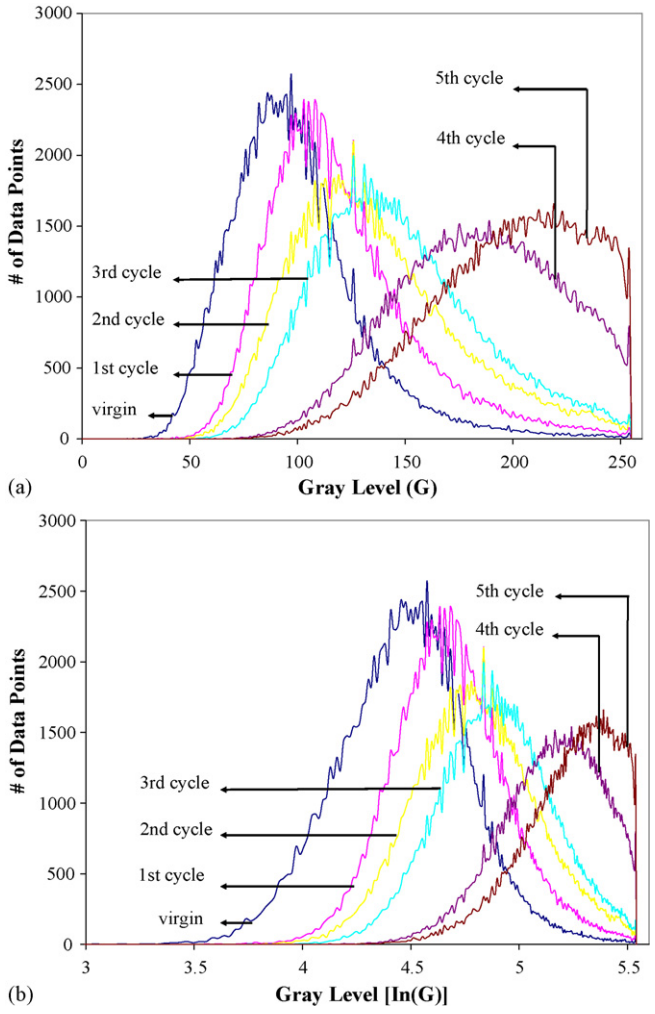

Fig. 11. Image histograms of thermoformed PMMA/ATH sample at 0.009 mm/s forming rate, 100 °C forming temperature (a) in gray level scale and (b) in logarithmic gray level scale.

thermoformed sample. Therefore, permanent stress whitening is hardly distinguishable in post-heated samples.

3.3. Stress whitening in thermoformed PMMA/ATH

At micro level, deformation in neat PMMA did not include any type void formation, and consequently stress whitening was not observed in deformed PMMA. However, PMMA/ATH samples displayed different levels of stress whitening at different thermoforming conditions. In optical images, increasing stress whitening level was observed as a change from darker to brighter appearance. SEM images of PMMA/ATH samples showed that light scattering entities on the surface were failure zones within and around ATH agglomerates. At forming temperatures below 100 °C, many densely packed cracks were present in ATH agglomerates, while combined particle disintegration and interfacial failure were dominant failure mechanisms at forming temperatures above 100 °C. Image histograms of optical images of PMMA/ATH samples thermoformed at 0.009 mm/s forming rate, 100 °C forming temperature are presented in Fig. 11. Increase in stress whitening is observed as a shift to higher gray values in histograms (Fig. 11a). Since total number of pixels is constant and same location is monitored in all optical images, higher stress whitening levels mean that pixels with small gray values in previous cycles have larger gray values in the following cycles.

For comparison of stress whitening at different thermoforming conditions, it is necessary to obtain an estimator from image histograms in Fig. 11a. It is possible to assume a Gaussian model for image histograms and define an estimator based on location parameter of Gaussian distribution. Gaussian model is a suitable model to fit histogram distributions in optical images, similar to magnetic resonance images [60]. Since gray level is in the range of 0–255, this distribution is truncated [61,62]. However, image histograms of virgin state and first three cycles (Fig. 11a) have long tails above mean (positive-skew) which may result in a biased estimator. Estimators in this form are inconvenient for comparison of stress whitening at different thermoforming cycles. In order to eliminate positive-skewness in data distributions, image histograms were plotted in natural logarithm of gray scale (Fig. 11b), which is one of the possible data reflection and data transformation techniques for obtaining normal distribution [63].

Image histograms plotted in natural logarithm of gray scale (Fig. 11b) display improvement in structure of distribution, such that central tendency of image histograms in logarithmic scale can be used for stress whitening quantification. Instead of mean value of distributions, a new estimator is defined in Equation (1), where N is total number of pixel points and n_i is number of pixel points corresponding to g_ith gray value. The proposed estimator uses only pixel points with gray values larger than some threshold value defined in Equation (2); thereby effect of outliers is minimized while all data points with high gray values are included in calculation of the index. In Equation (2), $\hat{\mu}_{\text{vir}}$ and $\hat{\sigma}_{\text{vir}}$ are mean and standard deviation of image histogram of virgin sample, respectively. Stress whitening is defined as the difference between index of kth thermoforming cycle and index of virgin state as shown in Equation (3).

$$G = \frac{\sum_{g_i \geq (\hat{\mu}-\hat{\sigma})_{\text{virgin}}} n_i \ln(g_i)}{N} \quad (1)$$

$$g_i \geq (\hat{\mu} - \hat{\sigma})_{\text{virgin}} \quad (2)$$

$$\Delta G = G^{k\text{th cycle}} - G^{\text{virgin}} \quad (3)$$

Stress whitening levels calculated for PMMA/ATH samples at different thermoforming conditions are presented in Fig. 12. At all forming temperatures and rates, stress whitening increases with increasing thermoforming cycle. Larger plastic deformation in successive thermoforming cycles results in formation and enlargement of more light scattering entities on the surface of PMMA/ATH which cause higher stress whitening level. On the other hand, forming rate and temperature control deformation mode in polymer matrix and micro-stress fields around ATH agglomerates which result in difference in stress whitening for the same level of deformation.

Stress whitening values at 0.9 and 0.09 mm/s forming rates can be categorized by two characteristic temperature of acrylic composite. At temperatures below 90 °C, thermal stress due to CTE mismatch becomes significant which influences stress field around ATH particles and at temperatures above glass transition temperature of PMMA (100 °C), polymer chain mobility increases compared to lower temperatures. At 0.9 mm/s forming rate (Fig. 12a), stress whitening values continuously increase from 75 °C forming temperature to 30 °C forming temperature under the influence of increased thermal stress due to CTE mismatch. Intensity of particle cracking observed in SEM images display close correlation with stress whitening levels at different forming temperatures. As forming temperature increases from 30 to 75 °C, density of particle cracks decreases and results in lower stress whitening (Fig. 7a–c). Similarly, higher density of particle cracks at 90 °C (Fig. 7d) compared to 75 °C (Fig. 7c) can be observed as an abrupt increase in stress whitening at 90 °C forming temperature compared to 75 °C (Fig. 12a). At 90 °C forming temperature, incompatible deformation

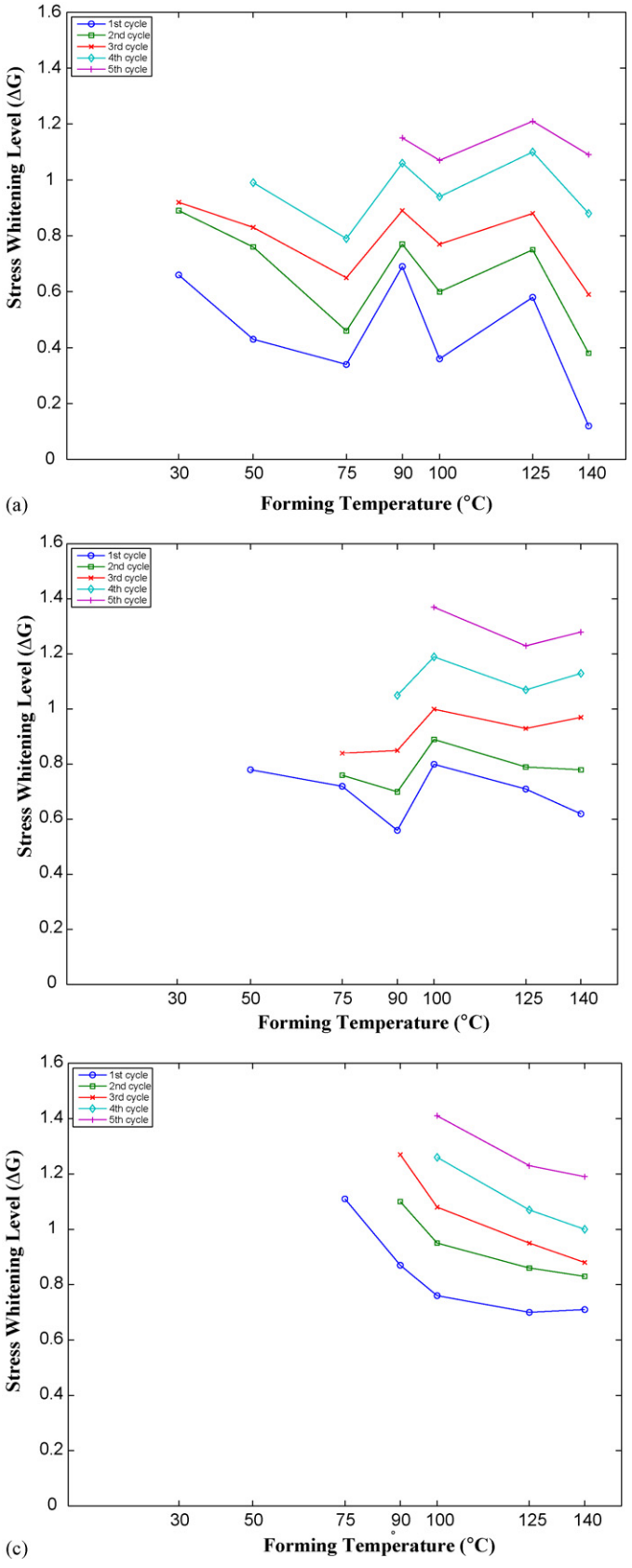

Fig. 12. Stress whitening, ΔG in thermoformed PMMA/ATH sample at (a) 0.9 mm/s, (b) 0.09 mm/s and (c) 0.009 mm/s forming rate.

capacities of constituents lead to significantly increased failure of ATH agglomerates compared to lower forming temperatures. Lower stress whitening values at 100 °C is primarily because of significantly reduced stiffness of PMMA. Increased stress whitening at 125 °C forming temperature is related to severe plastic deformation taking place in polymer matrix (Fig. 7f). At 140 °C forming temperature, increased surface irregularity due to sever plastic deformation of polymer matrix and particle disintegration type failure in ATH agglomerates (Fig. 7g) result in lower stress whitening compared to 125 °C (Fig. 12a).

At 0.09 mm/s forming rate (Fig. 12b), there is adequate time for specimens to reach thermal stability so that temperature sensitivity of stress whitening values can be classified simply into two regimes. At forming temperatures below 90 °C, stress whitening values increases as temperature decreases because of pronounced effect of thermal stress field around ATH particles. At forming temperatures above 100 °C, decreasing stress whitening with increasing forming temperature (Fig. 12b) is related to change in mode of microdeformation (Fig. 8c–e) compared to lower forming temperatures (Fig. 8a and b). At high-forming temperatures, flow-type deformation in polymer matrix and disintegration in ATH agglomerates reduce stress whitening significantly. Higher stress whitening level at 100 °C forming temperature compared to 90 °C forming temperature (Fig. 12b) is attributed to remarkable change in deformation behavior in polymer matrix inducing larger stress values around ATH particles.

At 0.009 mm/s forming rate (Fig. 12c), complete thermal stability of specimen is achieved before completion of forming step and slow forming rate allows reorganization of polymer chains. For all thermoforming cycles, change in gray level decreases as forming temperature increases. Relatively larger decrease in stress whitening between 75 and 90 °C is related to diminishing influence of thermal stress due to CTE mismatch while moderate decrease at higher temperatures is attributed to reduction in stiffness of polymer matrix. The transition in polymer matrix behavior at 100 °C forming temperature was suppressed at this forming rate causing less stress whitening compared to 90 °C forming temperature. SEM images show that voids formed by particle cracking is much larger at 100 °C forming temperature (Fig. 9c) than 90 °C forming temperature (Fig. 9b) which results in lower stress whitening. At 125 °C forming temperature (Fig. 9d), flow-type plastic deformation becomes significant in polymer matrix, while integrity of constituents is preserved at 140 °C forming temperature (Fig. 9e) producing lowest stress whitening at 0.009 mm/s forming rate.

4. Conclusions

A new experimental method is proposed to replicate conventional in situ heavy-gage thermoforming procedure. Effects of thermoforming conditions on material behavior through all stages and quality of final product can be studied via proposed experimental technique. At forming temperatures below 100 °C, behavior of the acrylic composites in forming stage is controlled by the competition between forming rate and cooling rate. Samples formed at faster rates have lower strength and stiffness compared to those formed at slower rates because of higher specimen temperature at high-forming rates. At forming temperatures above 100 °C, temperature dependency of stress–strain curves is less remarkable. Maximum experienced stress throughout thermoforming depends on stress relaxation and tensile stress induced by thermal shrinkage during dwell step. Stress relaxation is only significant at high-forming rates, whereas thermal stress is only observed at high-forming temperatures. Successive thermoforming cycles on same samples result in damage observed as material degradation in stress–strain curves. Even though, heat application prior to ther-

moforming cycles causes healing in the polymer matrix, failure in ATH agglomerates and filler-matrix interphase is irreversible. Coalescence and growth of previously formed cracks with increasing deformation level at each thermoforming cycle result in strength and stiffness degradation in PMMA/ATH samples. PMMA samples stretched to 50% strain did not display any void or crack formation on the surface. Contrary to some other researchers' observations, crazing is not observed in our PMMA and PMMA/ATH samples due to low-molecular weight of material and cross-linking agent present in the material. Tensile testing at temperatures around and above T_g of PMMA also results in homogenous drawing rather crazing type of yielding mechanism. Source of stress whitening observed in thermoformed acrylic composites is particle cracking and disintegration. At all forming temperatures and rates, stress whitening level increases with increasing thermoforming cycle due to the increase in density of light scattering entities. At low-forming temperatures, particle cracking was dominant deformation mechanism in thermoformed PMMA/ATH samples which resulted in higher stress whitening levels compared to higher forming temperatures. Surface micro-structure of thermoformed samples shows many densely packed cracks in ATH agglomerates. At high-forming temperatures, particle disintegration and interfacial failure were observed. SEM images of thermoformed samples show that nature of deformation in polymer matrix significantly changes with respect to forming temperature and rate leading to different modes of particle failure. The transition in mode of micro-deformation is around glass transition temperature (100 °C) of PMMA, above which deformation in polymer is more severe and flow-like. Large micro-deformation fields around ATH agglomerates cause particle disintegration instead of particle cracking at high temperatures. Flow-like polymer matrix deformation and particle disintegration at high-forming temperatures lower stress whitening. Small size and densely packed particle cracks formed at low-forming temperatures result in higher stress whitening compared to large size particle cracks observed at higher forming temperatures.

Acknowledgments

This project has been sponsored by DuPont Surface Corporation. Help received from Dr. Clyde Hutchins and Dr. Keith W. Pollak is appreciated.

Role of the funding source: DuPont Surface Corporation provided financial support for the conduct of the research; however, they were not involved in study design; in the collection, analysis and interpretation of data; in the writing of the report; and in the decision to submit the paper for publication.

References

[1] D. Rosato, Plastics Processing Data Handbook, Springer–Verlag, New York, 1997.
[2] J.L. Throne, Technology of Thermoforming, Hanser Publishers, New York, 1996.
[3] S.S. Morye, Polym. Eng. Sci. 45 (2005) 1369–1376.
[4] R.G. Jagger, A. Okdeh, J. Prosthet. Dent. 74 (1995) 542–545.
[5] M.J. Stephenson, M.E. Ryan, Polym. Eng. Sci. 37 (1997) 450–459.
[6] S.S. Morye, Polym. Eng. Sci. 45 (2005) 1377–1384.
[7] P.J. Dooling, C.P. Buckley, S. Rostami, N. Zahlan, Polymer 43 (2002) 2451–2465.
[8] D. Hylton, T. Spence, E. Sampson, K. Dorsey, R. Parker, T. Emyael, ANTEC 2000 Plast. 1 (2000) 804–821.
[9] C.W. Tan, E.M.A. Harkin-Jones, G.H. Menary, P.J. Martin, C.G. Armstrong, ANTEC 2005 Plast. 1 (2005) 1186–1191.
[10] H. Münstedt, S. Kurzbeck, J. Stange, Polym. Eng. Sci. 46 (2006) 1190–1195.
[11] Y. Dong, R.J.T. Lin, D. Bhattacharyya, J. Mater. Sci. 40 (2005) 399–410.
[12] Y. Dong, R.J.T. Lin, D. Bhattacharyya, Polym. Polym. Compos. 14 (2006) 307–328.
[13] D.V. Rosato, Plastics Institute of America Plastics Engineering, Manufacturing and Data Handbook, Kluwer Academic Publishers, Dordrecht, 2002.
[14] L.E. Nielsen, Mechanical Properties of Polymers and Composites, M. Dekker Inc., New York, 1974.
[15] A.J. Kinloch, R.J. Young, Fracture Behaviour of Polymers, Applied Science Publishers, London, 1983.
[16] H. Nathani, A. Dasari, R.D.K. Misra, Acta Mater. 52 (2004) 3217–3227.
[17] Q. Yuan, N. Ramisetti, R.D.K. Misra, Acta Mater. 56 (2008) 2089–2100.
[18] R. Hadal, H. Nathani, M. Tanniru, R.D.K. Misra, ANTEC 2005 Plast. 2 (2005) 1444–1448.
[19] R. Hadal, Q. Yuan, J.P. Jog, R.D.K. Misra, Mater. Sci. Eng. A 418 (2006) 268–281.
[20] R.D.K. Misra, R. Hadal, S.J. Duncan, Acta Mater. 52 (2004) 4363–4376.
[21] M.F. Mina, M.N.K. Chowdhury, A.K.M.M. Alam, G.H. Michler, Polym. Plast. Technol. Eng. 45 (2006) 217–222.
[22] M. Tanniru, R.D.K. Misra, Mater. Sci. Eng. A 424 (2006) 53–70.
[23] C. Chandavasu, M. Xanthos, K.K. Sirkar, C.G. Gogos, J. Plast. Film Sheet. 16 (2000) 288–300.
[24] A. Dasari, R.D.K. Misra, Acta Mater. 52 (2004) 1683–1697.
[25] R.D.K. Misra, H. Nathani, A. Dasari, S.D. Wanjale, J.P. Jog, Mater. Sci. Eng. A 386 (2004) 175–185.
[26] A. Mudaliar, Q. Yuan, R.D.K. Misra, Polym. Eng. Sci. 46 (2006) 1625–1634.
[27] D.L. Tillier, J. Meuldijk, G.W.H. Höhne, P.M. Frederik, O. Regev, C.E. Koning, Polymer 46 (2005) 7094–7108.
[28] C. Kilwon, J. Yang, E.P. Chan, Polymer 39 (1998) 3073–3081.
[29] L. Lalande, C.J.G. Plummer, J.-A.E. Månson, P. Gérard, Polymer 47 (2006) 2389–2401.
[30] C.J.G. Plummer, P. Béguelin, H.H. Kausch, Colloids Surf. A 153 (1999) 551–566.
[31] L. Lalande, C.J.G. Plummer, J.-A.E. Manson, P. Gérard, Eng. Fract. Mech. 73 (2006) 2413–2426.
[32] M. Tanniru, R.D.K. Misra, K. Berbrand, D. Murphy, Mater. Sci. Eng. A (2005) 208–220.
[33] A. Lazzeri, S.M. Zebarjad, M. Pracella, K. Cavalier, R. Rosa, Polymer 46 (2005) 827–844.
[34] R.S. Kody, D.C. Martin, Polym. Eng. Sci. 36 (1996) 298–304.
[35] A. Dasari, R.D.K. Misra, J. Rohrman, Polym. Eng. Sci. 44 (2004) 1738–1748.
[36] M. Wong, A. Moyse, F. Lee, H.J. Sue, J. Mater. Sci. 39 (2004) 3293–3308.
[37] J. Suwanprateeb, Polym. Plast. Technol. Eng. 39 (2000) 83–94.
[38] A. Dasari, Z.-Z. Yu, M. Yang, Q.-X. Zhang, X.-L. Xie, Y.-W. Mai, Compos. Sci. Technol. 66 (2006) 3097–3114.
[39] B. Finnigan, K. Jack, K. Campbell, P. Halley, R. Truss, P. Casey, D. Cookson, S. King, D. Martin, Macromolecules 38 (2005) 7386–7396.
[40] P. Hornsby, K. Premphet, J. Mater. Sci. 32 (1997) 4767–4775.
[41] O. Serenko, G. Goncharuk, S. Bazhenov, Dokl. Phys. 47 (2002) 822–824.
[42] C. Basaran, S. Nie, C. Hutchinson, H. Ergun, J. Mech. Behav. Mater. 17 (2006) 79–95.
[43] Q. Yuan, R.D.K. Misra, Polymer 47 (2006) 4421–4433.
[44] R.A. Ranade, J. Ding, S.L. Wunder, G.R. Baran, Compos. Part A Appl. Sci. Manuf. 37 (2006) 2017–2028.
[45] S. Nie, A micromechanical study of the damage mechanics of acrylic particulate composites under thermomechanical loading, Ph.D. Dissertation, Civil, Structural and Environmental Engineering, State University of New York at Buffalo, Buffalo, 2005.
[46] C. Basaran, S. Nie, C.S. Hutchins, H. Ergun, Int. J. Damage Mech. 17 (2008) 123–147.
[47] ASTM standard test for tensile properties of plastics, Annual Book of ASTM, vol. 08.01, 2008.
[48] US Patent 3,847,865, Use of aluminum trihydrate in a polymethyl methacrylate article.
[49] L. Mascia, Thermoplastics Materials Engineering, Elsevier Applied Science, London, New York, 1989.
[50] L.Z. Sun, H.T. Liu, Int. J. Solids Struct. 41 (2004) 2189–2203.
[51] R.P. Wool, K.M. O'Connor, Polym. Eng. Sci. 21 (1981) 970–977.
[52] W. Luo, C. Wang, R. Zhao, X. Tang, Y. Tomita, Mater. Sci. Eng., A 483–484 (2008) 580–582.
[53] W. Luo, W. Liu, Polym. Test. 26 (2007) 413–418.
[54] C.J.G. Plummer, P. Beguelin, H.H. Kausch, Polymer 37 (1996) 7–10.
[55] E. Kramer, in: H.H. Kausch, A.S. Argon (Eds.), Crazing in Polymers, Springer Berlin, Heidelberg, 1983.
[56] H.H. Kausch, J.L. Halary, C.J.G. Plummer, Macromol. Symp. 214 (2004) 17–30.
[57] C. Xiang, H.J. Sue, J. Chu, K. Masuda, Polym. Eng. Sci. 41 (2001) 23–31.
[58] C. He, A.M. Donald, M.F. Butler, Macromolecules 31 (1998) 158–164.
[59] J. Laatsch, G.M. Kim, G.H. Michler, T. Arndt, T. Sufke, Polym. Adv. Technol. 9 (1998) 716–720.
[60] Y. Wang, T. Adali, in: H. Yan (Ed.), Signal Processing for Magnetic Resonance Imaging and Spectroscopy, Marcel Dekker, Inc., New York, 2002, pp. 365–399.
[61] T. Adali, Y. Wang, in: L. Guan, S.Y. Kung, Jan Larsen (Eds.), Multimedia Image and Video Processing, CRC Press LLC, Boca Raton, 2001, pp. 201–242.
[62] T. Adali, Y. Wang, H. Li, in: Y.H. Hu, J. Hwang (Eds.), Handbook of Neural Network Signal Processing, CRC Press LLC, Boca Raton, 2002, pp. 12–21.
[63] T.N. Goh, M. Xie, X.Y. Tang, in: L.C. Tang, T.N. Goh, H.S. Yam, T. Yoap (Eds.), Six Sigma: Advanced Tools for Black Belts and Master Black Belts, John Wiley & Sons Inc., England, 2006, pp. 211–222.